PEA as a substitute for conventional invasive coronary angiography (16,19). Therefore, enhanced retrospective ECG-gated double volume 320-slice CT is appropriate for a routine CTPA protocol in CTEPH. In addition, more recent technical developments (e.g., prospective scan triggering during the systolic phase) could reduce the exposure dose in the future.

Sometimes motion artefacts or differences of density occurred at the junction point of the two gantry rotations. However, this did not affect the assessment of the morphology or the pulmonary arteries and heart. Furthermore, the breath-hold time was no more than 10 seconds with this modality, which would be beneficial in patients with CTEPH who may be unable to perform an extended breath hold required for MRI.

Technically, 64- or 16-slice helical, as well as 320-slice volume, ECG-gated enhanced CT can assess the morphology of the pulmonary arteries and right ventricle simultaneously. However they need several times more radiation exposure than 320-slice CT (32) and they also need at least 30 seconds of breath-hold time, which is difficult for CTEPH patients with reduced breath-hold capability. Thus it is difficult to use 64- or 16-slice CT for simultaneous clinical assessment of the pulmonary arteries and right ventricle.

Study limitations

First, this was a single centre retrospective study that included a small number of subjects. Therefore, further multicentre studies are needed in a larger, unselected

cohort of patients with suspected PH to evaluate whether 320-slice CT pulmonary angiography is as sensitive as V/Q lung scintigraphy to detect CTEPH. Second, not all subjects had different imaging modalities performed on the same day, so changes in hemodynamic conditions during the interval cannot be excluded. Third, the cine image with the most deformation of the septum was used to quantify IVS curvature, but this image may not correspond to the actual end of systole in all patients. This might contribute to some of the discordance observed between the 320-slice CT- and RHC-derived sPAP and PVR measurements. The discordance could not be neglected for evaluation of operative risk for CTEPH with high PVR, and RHC should remain mandatory until further improvement in the correlation is achieved. Fourth, only 18 of 44 patients underwent PEA and the remaining patients were not pathologically confirmed; however, similar results were observed in only surgically treated patients (the correlation coefficients of IVS curvature with sPAP and mPAP were -0.81 ($P<0.001$) and -0.83 ($P<0.001$), respectively). Fifth, although no patients developed worsening RV failure, 100 ml of contrast media and 50 ml of saline were injected for CT scanning, which may have increased RV volume.

Conclusions

The current study demonstrated that double volume retrospective ECG-gated 320-slice CT angiography allowed less invasive and simultaneous assessment of the morphology of the pulmonary arteries and pulmonary hemodynamics by the curvature of the IVS in CTEPH. Further investigation is necessary to ascertain whether this modality

can replace PDSA for the diagnosis of CTEPH and to determine whether IVS curvature can predict mortality in patients with CTEPH.

Acknowledgement

Author responsibilities:

Dr. Sugiura is the guarantor of this manuscript and contributed to the design of this study, data analysis, data interpretation and writing and review of the entire manuscript.

Dr. Tanabe contributed to image analysis, the data interpretation and critical review of the manuscript.

Dr. Matsuura contributed to image analysis, data analysis and data interpretation.

Dr. Shigeta contributed to image analysis, data analysis and data interpretation.

Dr. Kawata contributed to the data interpretation and critical review of the manuscript.

Dr. Juzyo contributed to the right heart catheterisation and invasive pulmonary digital subtraction angiography study.

Mr. Yanagawa contributed to the data interpretation and critical review of the manuscript.

Dr. Sakao contributed to the right heart catheterisation and invasive pulmonary digital subtraction angiography study.

Dr. Kasahara contributed to the right heart catheterisation and invasive pulmonary digital subtraction angiography study.

Prof. Tatsumi contributed to the data interpretation and critical review of the manuscript.

Funding Sources

This study was partly supported by a grant to the Respiratory Failure Research Group from the Ministry of Health, Labor and Welfare, Japan, and a grant from the Ministry of Education, Culture, Sports, Science and Technology of Japan (No 21590962 and 22590849).

References

1. Fedullo P, Kerr KM, Kim NH, Auger WR. Chronic thromboembolic pulmonary hypertension. Am J Respir Crit Care Med 2011;183:1605-1613.
2. Hoeper MM, Mayer E, Simonneau G, Rubin LJ. Chronic thromboembolic pulmonary hypertension. *Circulation* 2006;113:2011-2020.
3. Jamieson SW, Kapelanski DP, Sakakibara N, et al. Pulmonary endarterectomy: experience and lessons learned in 1500 cases. *Ann Thorac Surg* 2003;76:1457–1462.
4. Auger WR, Channick RN, Kerr KM, Fedullo PF. Evaluation of patients with suspected chronic thromboembolic pulmonary hypertension. *Semin Thorac Cardiovasc Surg* 1999;11:179-190.

5. Tunariu, N, Gibbs SJ, Win Z, et al. Ventilation-perfusion scintigraphy is more sensitive than multidetector CTPA in detecting chronic thromboembolic pulmonary disease as a treatable cause of pulmonary hypertension. J Nucl Med 2007;48:680-684.
6. Soler X, Kerr KM, Marsh JJ, et al. Pilot study comparing SPECT perfusion scintigraphy with CT pulmonary angiography in chronic thromboembolic pulmonary hypertension. Respirology 2012;17:180-184.
7. Willmann JK, Baumert B, Schertler T, et al. Aortoiliac and lower extremity arteries assessed with 16-detector row CT angiography: prospective comparison with digital subtraction angiography. *Radiology* 2005;236:1083-1093.
8. Pozzi-Mucelli F, Bruni S, Doddi M, et al. Detection of intracranial aneurysms with 64 channel multidetector row computed tomography: comparison with digital subtraction angiography. *Eur J Radiol* 2007;64:15-26.
9. Reichelt A, Hoeper MM, Galanski M, Keberle M. Chronic thromboembolic pulmonary hypertension: evaluation with 64-detector row CT versus digital substraction angiography. *Eur J Radiol* 2009;49-54.
10. Pitton MB, Kemmerich G, Herber S, et al. Chronic thromboembolic pulmonary hypertension: diagnostic impact of Multislice-CT and selective Pulmonary-DSA. *Rofo* 2002;174:474-479.
11. Ley S, Ley-Zaporozhan J, Pitton MB, et al. Diagnostic performance of state-of-the-art imaging techniques for morphological assessment of vascular abnormalities in patients with chronic thromboembolic pulmonary hypertension (CTEPH). Eur Radiol 2012; 22:607-616

12. Barst RJ, McGoon M, Torbicki A, et al. Diagnosis and differential assessment of pulmonary arterial hypertension. *J Am Coll Cardiol* 2004;43:40S–47S.

13. Raisinghani A, Ben-Yehuda O. Echocardiography in chronic thromboembolic pulmonary hypertension. *Semin Thorac Cardiovasc Surg*;2006:230-235.

14. Roeleveld RJ, Marcus JT, Faes TJ, et al. A. Interventricular septal configuration at MR imaging and pulmonary arterial pressure in pulmonary hypertension. *Radiology* 2005;234:710-717.

15. Taylor AJ, Cerqueira M, Hodgson JM, et al. ACCF/SCCT/ACR/AHA/ASE/ASNC/NASCI/SCAI/SCMR 2010 Appropriate Use Criteria for Cardiac Computed Tomography. A Report of the American College of Cardiology Foundation Appropriate Use Criteria Task Force, the Society of Cardiovascular Computed Tomography, the American College of Radiology, the American Heart Association, the American Society of Echocardiography, the American Society of Nuclear Cardiology, the North American Society for Cardiovascular Imaging, the Society for Cardiovascular Angiography and Interventions, and the Society for Cardiovascular Magnetic Resonance. *Circulation* 2010;122:e525-555.

16. Dewey M, Zimmermann E, Deissenrieder F, et al. Noninvasive coronary angiography by 320-row computed tomography with lower radiation exposure and maintained diagnostic accuracy: comparison of results with cardiac catheterization in a head-to-head pilot investigation. Circulation 2009; 120:867-875

17. Bajc M, Jonson B. Ventilation/Perfusion SPECT for Diagnosis of Pulmonary Embolism and Other Diseases. Int J Mol Imaging 2011; in press.

18. Moser KM, Fedullo PF, Finkbeiner WE, et al. Do patients with primary pulmonary hypertension develop extensive central thrombi? Circulation 1995; 91:741-745
19. Kim NH. Assessment of operability in chronic thromboembolic pulmonary hypertension. Proc Am Thorac Soc 2006; 3:584-588
20. Tanabe N, Sugiura T, Jujo T, et al. Subpleural perfusion as a predictor for a poor surgical outcome in chronic thromboembolic pulmonary hypertension. Chest 2012; 141: 929-934.
21. Coxson HO, Baile EM, King GG, et al. Diagnosis of subsegmental pulmonary emboli: a multi-center study using a porcine model. J Thorac Imaging 2005; 20:24-31
22. Baile EM, King GG, Muller NL, et al. Spiral computed tomography is comparable to angiography for the diagnosis of pulmonary embolism. Am J Respir Crit Care Med 2000; 161:1010-1015
23. Schoepf UJ, Costello P. CT angiography for diagnosis of pulmonary embolism: state of the art. Radiology 2004; 230:329-337
24. Diffin DC, Leyendecker JR, Johnson SP, et al. Effect of anatomic distribution of pulmonary emboli on interobserver agreement in the interpretation of pulmonary angiography. AJR Am J Roentgenol 1998; 171:1085-1089
25. Stein PD, Henry JW, Gottschalk A. Reassessment of pulmonary angiography for the diagnosis of pulmonary embolism: relation of interpreter agreement to the order of the involved pulmonary arterial branch. Radiology 1999; 210:689-691
26. King ME, Braun H, Goldblatt A, Liberthson R, Weyman AE. Interventricular septal configuration as a predictor of right ventricular systolic hypertension in children: a cross-sectional echocardiographic study. *Circulation* 1983;68:68-75

27. Riedel M, Stanek V, Widimsky J, et al. Longterm follow-up of patients with pulmonary thromboembolism. Late prognosis and evolution of hemodynamic and respiratory data. Chest 1982; 81:151-158
28. Lewczuk J, Piszko P, Jagas J, et al. Prognostic factors in medically treated patients with chronic pulmonary embolism. Chest 2001; 119:818-823
29. Saouti N, de Man F, Westerhof N, et al. Predictors of mortality in inoperable chronic thromboembolic pulmonary hypertension. Respir Med 2009; 103:1013-1019
30. Ishida K, Masuda M, Tanabe N, et al. Long-term outcome after pulmonary endarterectomy for chronic thromboembolic pulmonary hypertension. J Thorac Cardiovasc Surg 2011
31. Corsico AG, D'Armini AM, Cerveri I, et al. Long-term outcome after pulmonary endarterectomy. Am J Respir Crit Care Med 2008; 178:419-424
32. Bischoff B, Hein F, Meyer T, et al. Comparison of sequential and helical scanning for radiation dose and image quality: results of the Prospective Multicenter Study on Radiation Dose Estimates of Cardiac CT Angiography (PROTECTION) I Study. *Am J Roentgenol* 2010;194:1495-1499
33. Rybicki FJ, Otero HJ, Steigner ML, et al. Initial evaluation of coronary images from 320-detector row computed tomography. Int J Cardiovasc Imaging 2008; 24:535-546
34. Diekmann S, Siebert E, Juran R, et al. Dose exposure of patients undergoing comprehensive stroke imaging by multidetector-row CT: comparison of 320-detector row and 64-detector row CT scanners. AJNR Am J Neuroradiol 2010; 31:1003-1009
35. Silverman JD, Paul NS, Siewerdsen JH. Investigation of lung nodule detectability in low-dose 320-slice computed tomography. Med Phys 2009; 36:1700-1710

36. Kroft LJ, Roelofs JJ, Geleijns J. Scan time and patient dose for thoracic imaging in neonates and small children using axial volumetric 320-detector row CT compared to helical 64-, 32-, and 16- detector row CT acquisitions. Pediatr Radiol 2010; 40:294-300

37. Yamashiro T, Miyara T, Takahashi M, et al. Lung Image Quality with 320-row Wide-volume CT Scans: The Effect of Prospective ECG-gating and Comparisons with 64-row Helical CT Scans. Acad Radiol 2012; 19:380-388

FIGURE LEGENDS

Figure 1. The method of calculating interventricular septal curvature. (A) Short-axis cine images of the heart were acquired using double oblique multiplanar reformation. The interventricular septal curvature was measured in the short-axis image plane at the midventricular level (at least one papillary muscle visible). At this level, the cine image with the most deformation of the septum (at 35% of R-R interval in this case) was used for quantification. (B) Three points at the anterior, middle, and posterior positions on the interventricular septum were marked and the X and Y coordinates were read. (C) A

circle which passed through the three points on the septum was used to calculate the radius of curvature of the septum. A rightward (physiologic) curvature was denoted as a positive value, and a leftward curvature as a negative value. (Window/Centre settings were 600/150 HU)

IVS= interventricular septum

Figure 2. Bland-Altman plot shows interobserber variability for measurements of interventricular septal curvature. The average value of the two measurements is plotted along the x-axis; the difference is plotted along the y-axis. The solid line represents the mean value of the differences in measurements between the two observers (-0.01 cm^{-1}, 95% confidence intervals: -0.03, 0.02 cm^{-1}). The upper and the lower dashed lines represent the limits of agreement, calculated as the mean ± 1.96 standard deviation (-0.17, 0.15 cm^{-1}).

SD= standard deviation

Figure 3. Correlation between interventricular septal curvature obtained by 320-slice CT and sPAP based on right heart catheterisation. The scatterplot shows the strong relation between interventricular septal curvature and sPAP ($r=-0.79$, $p<0.001$, $n=44$). The solid line represents the regression line with a slope of -74.368 and a y-intercept of 74.518. The dotted lines represent the upper and the lower 95% confidence intervals for the limits of regression.

CT= computed tomography, sPAP= systolic pulmonary artery pressure

Figure 4. Correlation between interventricular septal curvature obtained by 320-slice CT and mPAP by right heart catheterisation. The scatterplot shows the strong relation between interventricular septal curvature and mPAP ($r=-0.86$, $p<0.001$, $n=44$). The solid line represents the regression line with a slope of -41.519 and a y-intercept of 41.969. The dotted lines represent the upper and lower 95% confidence interval for the limits of regression.

CT= computed tomography, mPAP= mean pulmonary artery pressure

Table 1. Clinical and hemodynamics information of the study population

N=44	Mean±SD
Age (years)	59.2±11.3
Gender (female/male)	28/16 (64%/36%)
WHO(1/2/3/4)	1/17/22/4
	(2%/39%/50%/9%)
Right Heart Catheterization	
Mean pulmonary artery pressure (mPAP) (mmHg)	42.2±9.9
Systolic pulmonary artery pressure (sPAP) (mmHg)	70.4±19.3
Cardiac output (CO) (L/min)	4.17±0.89
Cardiac index (CI) (L/min/m^3)	2.54±0.47
Pulmonary vascular resistance (PVR) (dynes · s · cm^{-5})	696±274
(Wood units)	8.72±3.43

Values represent mean±standard deviation unless otherwise indicated.

Definition of abbreviations; WHO=World Health Organization functional classes,

SD=standard deviation

Table 2. Summary of pathological vascular findings as delineated by CTPA and PDSA, and statistical analysis of findings in CTPA compared to findings in PDSA

	CTPA	PDSA	Sensitivity	Specificity	PPV	NPV	K(95%CI)
Main/lobar arteries (N=344)			(%)	(%)	(%)	(%)	
Number of normal vessels	271	277					
Chronic thromboembolic findings	73	67	97.0	97.1	89.0	99.3	0.91(0.86-0.96)
Segmental arteries (N=860)							
Number of normal vessels	661	670					
Chronic thromboembolic findings	199	190	85.8	94.6	81.9	95.9	0.79(0.74-0.84)

Definition of abbreviations; CTPA= Pulmonary angiography on 320-slice CT, PDSA= pulmonary digital subtraction angiography, PPV=positive predictive value, NPV=negative predictive value, K=Cohen's Kappa, 95%CI=95% confidence interval

Figure 1

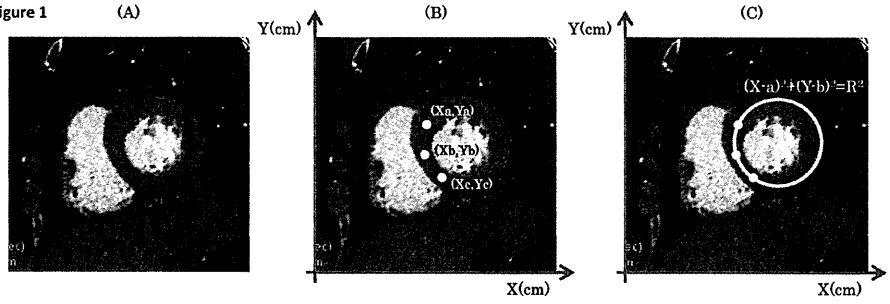

The method of calculating interventricular septal curvature. (A) Short-axis cine images of the heart were acquired using double oblique multiplanar reformation. The interventricular septal curvature was measured in the short-axis image plane at the midventricular level (at least one papillary muscle visible). At this level, the cine image with the most deformation of the septum (at 35% of R-R interval in this case) was used for quantification. (B) Three points at the anterior, middle, and posterior positions on the interventricular septum were marked and the X and Y coordinates were read. (C) A circle which passed through the three points on the septum was used to calculate the radius of curvature of the septum. A rightward (physiologic) curvature was denoted as a positive value, and a leftward curvature as a negative value. (Window/Centre settings were 600/150 HU)
IVS= interventricular septum
600x200mm (96 x 96 DPI)

Figure 2

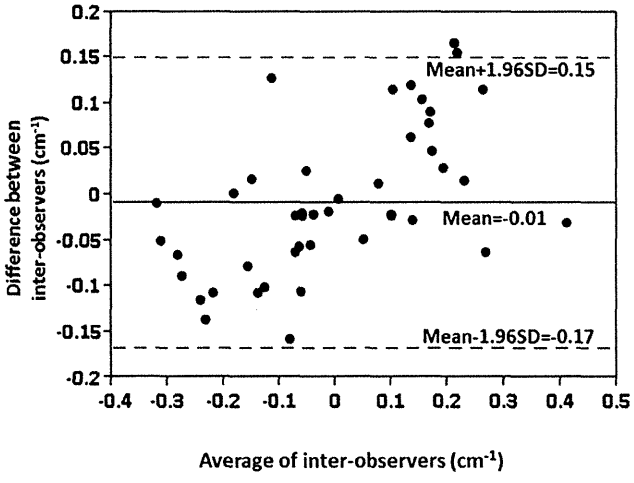

Bland-Altman plot shows interobserber variability for measurements of interventricular septal curvature. The average value of the two measurements is plotted along the x-axis; the difference is plotted along the y-axis. The solid line represents the mean value of the differences in measurements between the two observers (-0.01 cm-1, 95% confidence intervals: -0.03, 0.02 cm-1). The upper and the lower dashed lines represent the limits of agreement, calculated as the mean ± 1.96 standard deviation (-0.17, 0.15 cm-1).
SD= standard deviation
254x190mm (96 x 96 DPI)

Figure 3

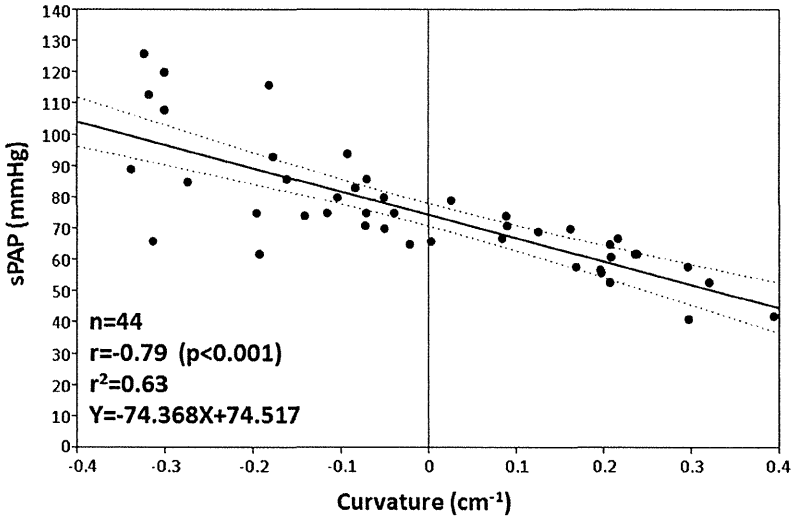

Correlation between interventricular septal curvature obtained by 320-slice CT and sPAP based on right heart catheterisation. The scatterplot shows the strong relation between interventricular septal curvature and sPAP ($r=-0.79$, $p<0.001$, $n=44$). The solid line represents the regression line with a slope of -74.368 and a y-intercept of 74.518. The dotted lines represent the upper and the lower 95% confidence intervals for the limits of regression.
CT= computed tomography, sPAP= systolic pulmonary artery pressure

254x190mm (96 x 96 DPI)

Figure 4

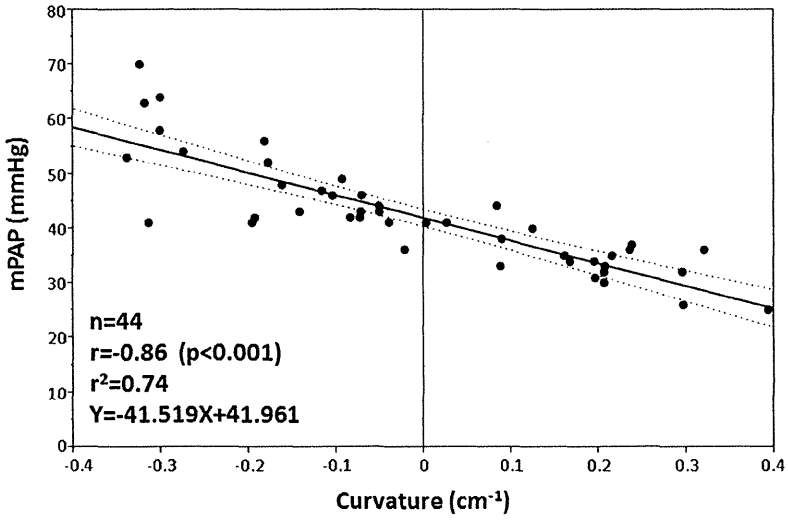

Correlation between interventricular septal curvature obtained by 320-slice CT and mPAP by right heart catheterisation. The scatterplot shows the strong relation between interventricular septal curvature and mPAP ($r=-0.86$, $p<0.001$, $n=44$). The solid line represents the regression line with a slope of -41.519 and a y-intercept of 41.969. The dotted lines represent the upper and lower 95% confidence interval for the limits of regression.
CT= computed tomography, mPAP= mean pulmonary artery pressure

254x190mm (96 x 96 DPI)

Research Article

Metabolomic analysis of bone morphogenetic protein receptor type 2 mutations in human pulmonary endothelium reveals widespread metabolic reprogramming

Joshua P. Fessel[1], Rizwan Hamid[2], Bryan M. Wittmann[3], Linda J. Robinson[1], Tom Blackwell[1], Yuji Tada[1], Nobuhiro Tanabe[4], Koichiro Tatsumi[4], Anna R. Hemnes[1], and James D. West[1]

[1]Department of Medicine, Division of Allergy, Pulmonary, and Critical Care Medicine, Vanderbilt University, Nashville, Tennessee, USA, [2]Department of Pediatrics, Vanderbilt University, Nashville, Tennessee, USA, [3]Metabolon, Durham, North Carolina, USA, [4]Department of Respirology (B2), Graduate School of Medicine, Chiba University, Chiba, Japan

ABSTRACT

Pulmonary arterial hypertension (PAH) is a progressive and fatal disease of the lung vasculature for which the molecular etiologies are unclear. Specific metabolic alterations have been identified in animal models and in PAH patients, though existing data focus mainly on abnormalities of glucose homeostasis. We hypothesized that analysis of the entire metabolome in PAH would reveal multiple other metabolic changes relevant to disease pathogenesis and possible treatment. Layered transcriptomic and metabolomic analyses of human pulmonary microvascular endothelial cells (hPMVEC) expressing two different disease-causing mutations in the bone morphogenetic protein receptor type 2 (BMPR2) confirmed previously described increases in aerobic glycolysis but also uncovered significant upregulation of the pentose phosphate pathway, increases in nucleotide salvage and polyamine biosynthesis pathways, decreases in carnitine and fatty acid oxidation pathways, and major impairment of the tricarboxylic acid (TCA) cycle and failure of anaplerosis. As a proof of principle, we focused on the TCA cycle, predicting that isocitrate dehydrogenase (IDH) activity would be altered in PAH, and then demonstrating increased IDH activity not only in cultured hPMVEC expressing mutant BMPR2 but also in the serum of PAH patients. These results suggest that widespread metabolic changes are an important part of PAH pathogenesis, and that simultaneous identification and targeting of the multiple involved pathways may be a more fruitful therapeutic approach than targeting of any one individual pathway.

Key Words: pulmonary arterial hypertension, BMPR2, Warburg effect, anaplerosis, isocitrate dehydrogenase

Pulmonary arterial hypertension (PAH) is a fatal, progressive disease of the pulmonary vasculature characterized by increasing pulmonary vascular resistance that leads to right heart failure and death.[1,2] The disease exists in several forms in humans, including a heritable form caused primarily by mutations in bone morphogenetic protein receptor type 2 (BMPR2) and an idiopathic form that is clinically and in many ways molecularly indistinguishable from the inherited disease.[3-5] Despite extensive investigations in PAH patients and in a variety of animal models of PAH, the molecular mechanisms of disease pathogenesis have remained relatively obscure. Multiple converging lines of evidence point to disruption of interdependent metabolic pathways as being central to the molecular pathogenesis of PAH. In expression arrays from Bmpr2 mutant mice, nearly 50% of the significantly altered genes fall into metabolic gene ontology groups, without identification of specific metabolic pathways.[6] Several animal models of PAH

Address correspondence to:
Dr. Joshua P. Fessel
Vanderbilt University
Department of Medicine, Division of Allergy
Pulmonary, and Critical Care Medicine
1161 21st Avenue South, MCN Suite T1218
Nashville, TN 37232, USA
Email: joshua.p.fessel@vanderbilt.edu

Access this article online

Quick Response Code:	Website: www.pulmonarycirculation.org
	DOI: 10.4103/2045-8932.97606
	How to cite this article: Fessel JP, Hamid R, Wittmann BM, Robinson LJ, Blackwell T, Tada Y et al. Metabolomic analysis of bone morphogenetic protein receptor type 2 mutations in human pulmonary endothelium reveals widespread metabolic reprogramming. Pulm Circ 2012;2:201-13.

show a shift toward aerobic glycolysis, the so-called "Warburg effect" that has been identified as central to malignant transformation in a number of tumor types.[7-9] Alterations in glucose uptake and utilization, alongside changes in mitochondrial oxidative phosphorylation, have been demonstrated in the pulmonary artery endothelium from patients with PAH.[10,11] More recently, PAH patients not previously known to have diabetes or any other obvious metabolic diseases were found to have measurable increases in hemoglobin A1c compared to age- and BMI-matched controls, suggesting that whole-body glucose homeostasis is impaired in PAH.[12,13] Pulmonary hypertension associated with chronic hypoxia has been directly linked to an imbalance between glycolysis, glucose oxidation, and fatty acid oxidation.[9] Finally, therapies aimed at normalizing glucose oxidation directly (e.g., inhibitors of pyruvate dehydrogenase kinase such as dichloroacetate) or via modulation of the balance between fatty acid oxidation and glucose oxidation (e.g., partial fatty acid oxidation inhibitors such as trimetazidine or ranolazine) have shown great promise in treating PAH and have demonstrated the importance of metabolic disturbances in disease initiation and maintenance.[8,14-18] Indeed, dichloroacetate has entered Phase I trials in humans (ClinicalTrials.gov identifier NCT01083524). Though the weight of evidence suggests that metabolic reprogramming is a key feature of the molecular pathogenesis of PAH, existing data focus mainly on abnormalities of glucose homeostasis, and the full breadth and scope of the altered metabolic pathways in PAH are unknown.

We hypothesized that a broad-based metabolomic analysis of BMPR2 mutations that are known to cause PAH would reveal multiple coexisting and interdependent metabolic abnormalities beyond changes in glucose homeostasis. We quantify several hundred small molecule metabolites in native human pulmonary microvascular endothelial cells (hPMVEC) and in hPMVEC expressing one of two different disease-causing BMPR2 mutations. Organization of the significantly changed metabolites into known biochemical pathways confirms that multiple interconnected metabolic pathways are deranged in PAH. Gene expression array analysis from these same cells shows that metabolic genes represent the largest single group of significantly changed genes and support the findings from the metabolomic analyses. Using these layered metabolomic and transcriptomic analyses, we then predict alteration of the activity of a specific enzyme in the tricarboxylic acid (TCA) cycle – namely, isocitrate dehydrogenase (IDH) — as a proof of principle and demonstrate increased IDH activity in mutant hPMVEC and in the serum of patients with PAH.

MATERIALS AND METHODS

Human pulmonary microvascular endothelial cell culture

Human PMVEC were grown in culture as previously described.[19-21] Cells were maintained in Endothelial Cell Growth Medium MV from PromoCell (Heidelberg, Germany) in standard cell culture incubators (37°C, humidified, 5% CO_2) and were used at or before the 10th passage.

Generation of stably transfected hPMVEC

Cells were transfected with either empty vector (native) or vector containing BMPR2 with R332X (KD) or 2579-2580delT (CD) mutations and stably selected using G418S as previously described.[22] Endothelial character of the cells for this study was confirmed by immunohistochemistry for the von Willebrand factor and by analysis of expression arrays for a panel of endothelial markers (Figure S1A, B).

Transcriptomic analysis

Native and mutant hPMVEC were grown to 80% confluence, transitioned from G418S selection for at least 12 hours, and mRNA was isolated as described.[23] Two Affymetrix HGU133 Plus 2 arrays were run for each condition, with RNA for each array representing a pool of three independently grown plates, for a total of six arrays representing 18 biologically distinct events (three conditions × three plates × two arrays each). Results were analyzed using dChip and R statistical software. Significantly changed genes were determined using a requirement of a minimum of a 2× change, a minimum difference in expression of at least 200 arbitrary Affymetrix units, and a $P<0.01$ by a t-test for differences.

Metabolomic analysis

Full details of the methodology for the mass spectrometry-based metabolomic analyses are given in Supplemental Methods and as described previously.[24,25] Briefly, samples (N=7 for each condition) were subjected to methanol extraction, split into aliquots for analysis by ultrahigh performance liquid chromatography/mass spectrometry (UHPLC/MS) in either the positive or negative ion mode or by gas chromatography/mass spectrometry (GC/MS). Internal standards and controls for signal blank, technical replicates, and instrument performance were spiked into the samples and tracked throughout the analysis. Metabolite concentrations were determined by automated ion detection, manual visual curation, and were analyzed in-line using software developed by Metabolon.[26] Significance was set at $P<0.05$ by Welch's two-sample t-test with correction for multiple comparisons using q-values.[27]

$NADP^+$-dependent IDH activity assays

IDH activity assays were performed using the BioVision Isocitrate Dehydrogenase Activity Assay Kit (Mountain

View, Calif.) according to the manufacturer's instructions. For hPMVEC, cells were grown in 6-well plates to 50—60% confluence to yield approximately 500,000 cells per well, harvested, and lysed directly in the assay buffer. Aliquots were used for the IDH activity assay and for protein concentration determination by Pierce BCA assay. For serum, samples were used as undiluted 50 μl aliquots and assayed for IDH activity according to the instructions.

Human subjects

All patients and normal volunteers provided written informed consent to participate in research protocols approved by the institutional review boards of all participating institutions (IRB protocol number 9401). Blood was drawn by standard venipuncture, centrifuged to collect serum, and serum was stored at −80°C until analysis.

Statistical analyses

Analyses were performed using R statistical software and using GraphPad Prism. Welch's t-test or two-way ANOVA were used for tests of statistical significance. Box-and-whisker plots represent 25th—75th percentiles with the box, the median with the center line, and Tukey whiskers representing 1.5 times the interquartile range. Scatter plots show individual data points with mean±SEM depicted. For most analyses, significance was set at $P<0.05$, with $P<0.01$ being used as the significance threshold for RNA expression microarray analysis.

RESULTS

BMPR2 mutations resulted in widespread changes in endothelial cell gene expression that organized into specific pathways

We sought to compare expression arrays from native hPMVEC to those from hPMVEC expressing one of two mutant BMPR2 constructs, and to organize the significantly different genes into functional pathways. Human pulmonary microvascular endothelial cells were stably transfected with either R332X mutation in the kinase domain (KD) or a 2579-2580delT mutation in the cytoplasmic tail domain (CD). The CD mutation has been previously shown to dysregulate BMPR2 interaction with and signaling through LIMK-1, c-Src, and Tctex-1;[28-31] the KD mutation also includes dysregulated signaling through the canonical Smad pathway.[32]

Using a requirement of a minimum of twofold change, a minimum difference in expression of at least 200 arbitrary Affymetrix units, and a $P<0.01$ by t-test for difference, we found 687 probe sets representing 507 unique Entrez IDs, with common changes between both BMPR2 mutants and native hPMVEC, with a false discovery rate (FDR) of zero (determined by scrambling group identifiers). These data have been deposited in GEO, accession number pending , and a full list of the 507 genes is provided in Supplemental Dataset S1. Distribution of gene ontology groups was nearly identical to our previously published expression arrays interrogating PMVEC isolated from our $Bmpr2^{R899X}$ and $Bmpr2^{delx4+}$ mouse models.[6,33,34] These included genes involved in apoptosis, proliferation, stimulus response, cytoskeletal organization, and development (Fig. 1). Roughly 40% of the genes changed (216/507) were related to small molecule metabolism. Heterologous expression of BMPR2 mutations resulted in broad changes in TCA cycle, glycolysis, hypoxia-inducible factor (HIF) responsive metabolic elements, and carnitine, fatty acid, and glutamate metabolism compared to expression of native BMPR2. Relatively unaffected pathways include glycan synthesis and metabolism, vitamin/cofactor metabolism (with the exception of folate and single-carbon metabolism), and xenobiotic metabolism. Thus, the affected pathways showed a degree of specificity as opposed to nonspecific whole metabolome dysfunction.

Metabolomic analysis of BMPR2 mutant endothelial cells showed significant alteration of multiple interdependent metabolic pathways

To determine the whole metabolome consequences of disease-causing BMPR2 mutation in endothelial cells, we undertook a simultaneous multiplexed mass spectrometric quantification of several hundred small molecule metabolites in CD and KD mutant hPMVEC and compared these mutations to the native hPMVEC. In this analysis, 267 small molecule metabolites were confidently identified in seven biological replicates for each condition described above (native, CD, and KD, Figure S2). Significantly changed biochemicals from the native condition were identified as those biochemicals with a P-value <0.05 based upon Welch's two-sample t-test, which had a maximum FDR of 3.2% based upon q-values[27] for that set of biochemicals with P-values <0.05. The full dataset is provided in Supplemental Dataset S2. Compared to the native hPMVEC, the CD mutants showed significant changes in 65% of the metabolites quantified (172/267, with 87 increased and 85 decreased) and the KD mutants showed significant changes in 37% of the metabolites (99/267, with 61 increased and 38 decreased). This represented confident identification of approximately 11% of the database of named compounds available in this analysis, with the CD mutants showing significant changes in the levels of approximately 7% of the total compounds in the database. For the KD mutants, a further 14% (38 metabolites) approached statistical significance ($0.05<P<0.10$ by Welch's two-sample t-test), though these were not included in the analyses discussed below.